Talanta 103 (2013) 322–329

Contents lists available at SciVerse ScienceDirect

Talanta

journal homepage: www.elsevier.com/locate/talanta

A novel enzyme-free amperometric sensor for hydrogen peroxide based on Nafion/exfoliated graphene oxide–Co_3O_4 nanocomposite

Ali A. Ensafi *, M. Jafari–Asl, B. Rezaei

Department of Chemistry, Isfahan University of Technology, Isfahan 84156–83111, Iran

ARTICLE INFO

Article history:
Received 13 August 2012
Received in revised form
18 October 2012
Accepted 20 October 2012
Available online 27 October 2012

Keywords:
Hydrogen peroxide
Nafion/exfoliated graphene oxide–Co_3O_4 nanocomposite
Cyclic voltammetry and amperometry

ABSTRACT

Electrochemical detection of H_2O_2 was investigated on a Nafion/exfoliated graphene oxide/Co_3O_4 nanocomposite (Nafion/EGO/Co_3O_4) coated glassy carbon electrode. The morphological characterization was examined by scanning electron microscopy, X-ray diffraction, and electrochemical impedance spectroscopy. The modified electrode showed well defined and stable redox couples signal in both alkaline and natural aqueous solutions with excellent electrocatalytic activity for oxidation of hydrogen peroxide. The response of the modified electrode to H_2O_2 was examined using amperometry (at 0.76 V vs. Ag/AgCl reference electrode) in a phosphate buffer solution (pH 7.4). The detection limit was 0.3 μmol L^{-1} with a linearity of up to four orders of magnitude and a sensitivity of 560 μA $mmol^{-1}$ L cm^{-2}. The response time of the electrode to achieve 95% of the steady-state current was recorded at 4 s. The ability of the sensor for routine analyses was demonstrated by the detection of H_2O_2 presents in milk samples with appreciable recovery values. In addition, the Nafion/EGO/Co_3O_4-GCE showed good selectivity for H_2O_2 detection in the presence of ascorbic acid, uric acid, and glucose. The attractive analytical performances such as remarkable catalytic activity, good reproducibility, long term stability, and facile preparation method made this novel nanocomposite electrode promising for the development of effective H_2O_2 sensor.

1. Introduction

Hydrogen peroxide is a by-product of the reactions catalyzed by large numbers of oxidase enzymes [1]. It is essential for clinical, chemical, and biological applications as well as in food production, pulp and paper bleaching, and sterilization, among others. Furthermore, hydrogen peroxide and its derivatives are powerful oxidizing agents, a property that has found them extensive applications in the synthesis of many organic compounds. The detection of H_2O_2, therefore, is of vital importance in environmental, clinical, and pharmaceutical analyses [2]. Many techniques including spectrometry, titrimetry, and chemiluminescence have been employed for the determination of H_2O_2 [3–6], which are generally time-consuming, highly prone to interferences [7], and difficult for automated detection. Hence, the methods are unreliable for detection in food and biological samples due to the difficulty of obtaining clear solutions for final measurements. Electrochemical methods [8–11] can overcome the above drawbacks for the determination of H_2O_2 owing to their advantages of easy preparation, fast detection, low consumption, and high selectivity and sensitivity [12]. Direct electrochemical reduction or oxidation of H_2O_2 at ordinary solid electrodes is, however, a slow process that requires a large overpotential, posing a major barrier against the determination of H_2O_2 [13–16]. An efficient approach to overcome this problem is to modify the bare electrode with suitable electrocatalyst that can reduce the high overpotential for H_2O_2 reduction or oxidation [17,18]. In order to decrease the overpotential and increase electron transfer kinetics, several enzyme-based electrochemical biosensors were developed with such enzymes as horseradish peroxidase (HRP) [19], cytochrome c [20], and hemoglobin [21] as the active site. Unfortunately, the enzyme-based detection methodologies are often complicated, expensive, and time consuming. Moreover, several precautions should be taken to overcome the enzyme's instability and temperature effects [22,23]. Many enzyme-free sensors utilizing metals or metal oxide nanoparticles such as silver [24], platinum [25], gold [26], iridium oxide films [27,28], rhodium [29], indium-tin oxide [30], and ruthenium [31] have been entertained as a remedy for the successful determination of hydrogen peroxide.

Cobalt oxide-based materials have been widely used for electrocatalytic activity toward various compounds, such as hydroquinone [32] and methanol [33]. A novel and fascinating carbon material used as a new substitute for these materials is graphene, a single layer of carbon atoms in a closely packed

* Corresponding author. Tel.: +98 311 3913269; fax: +98 311 3912350.
E-mail addresses: Ensafi@cc.iut.ac.ir, ensafi2009@gmail.com, ensafi@yahoo.com (A.A. Ensafi).

0039-9140/$ - see front matter © 2012 Elsevier B.V. All rights reserved.
http://dx.doi.org/10.1016/j.talanta.2012.10.063

honeycomb two-dimensional lattice, which has recently attracted much attention from both experimental and theoretical scientific communities due to its many unique and excellent properties [34–36].

Herein, we report an enzyme-free amperometric sensor based on nano-sized active cobalt oxide species decorated on graphene. The electrochemical properties of Nafion/exfoliated graphene oxide/Co_3O_4 nanocomposite modified glassy carbon electrode (Nafion/EGO/Co_3O_4 – GCE), including stability, solution pH, and kinetic parameters of the redox active composite have been evaluated by electrochemical techniques. The electrocatalytic activity of the modified electrode for the oxidation of hydrogen peroxide has also been investigated and its possible analytical applications have been explored by using the modified electrode for amperometric detection of hydrogen peroxide.

2. Experimental

2.1. Reagents

H_2O_2 solution (30%), $Co(NO_3)_6$, graphite and Nafion (5% in a mixture of lower aliphatic alcohols and water) were purchased from Merck. All other chemicals were of analytical grade and used without further purification. Stock standard solution of H_2O_2 was prepared fresh every day in doubly distilled water. Solutions with lower concentrations were prepared by diluting with doubly distilled water and used within a few hours. Phosphate buffer solutions (PBS) (0.1 mol L^{-1}) were prepared from H_3PO_4 and NaOH.

2.2. Apparatus

A μ–Autolab electrochemical analyzer, Model PGSTAT-30 potentiostat, galvanostat (Eco–Chemie, the Netherlands), controlled by a microcomputer was used for all voltammetric and amperometric measurements. Data were acquired and processed (background correction) using the GPSE computrace software 4.9.007. A standard three-electrode cell containing a platinum wire auxiliary electrode, a saturated Ag/AgCl reference electrode, and a Nafion/EGO–Co_3O_4–GCE as a working electrode were employed for the electrochemical studies. A pH–meter (Corning, Model 140) with a double junction glass electrode was used to check the pH levels of the solutions.

Scanning electron microscopy (SEM) was accomplished on a PHILIPS XL–30 ESEM at an accelerating voltage of 20 kV. X–ray

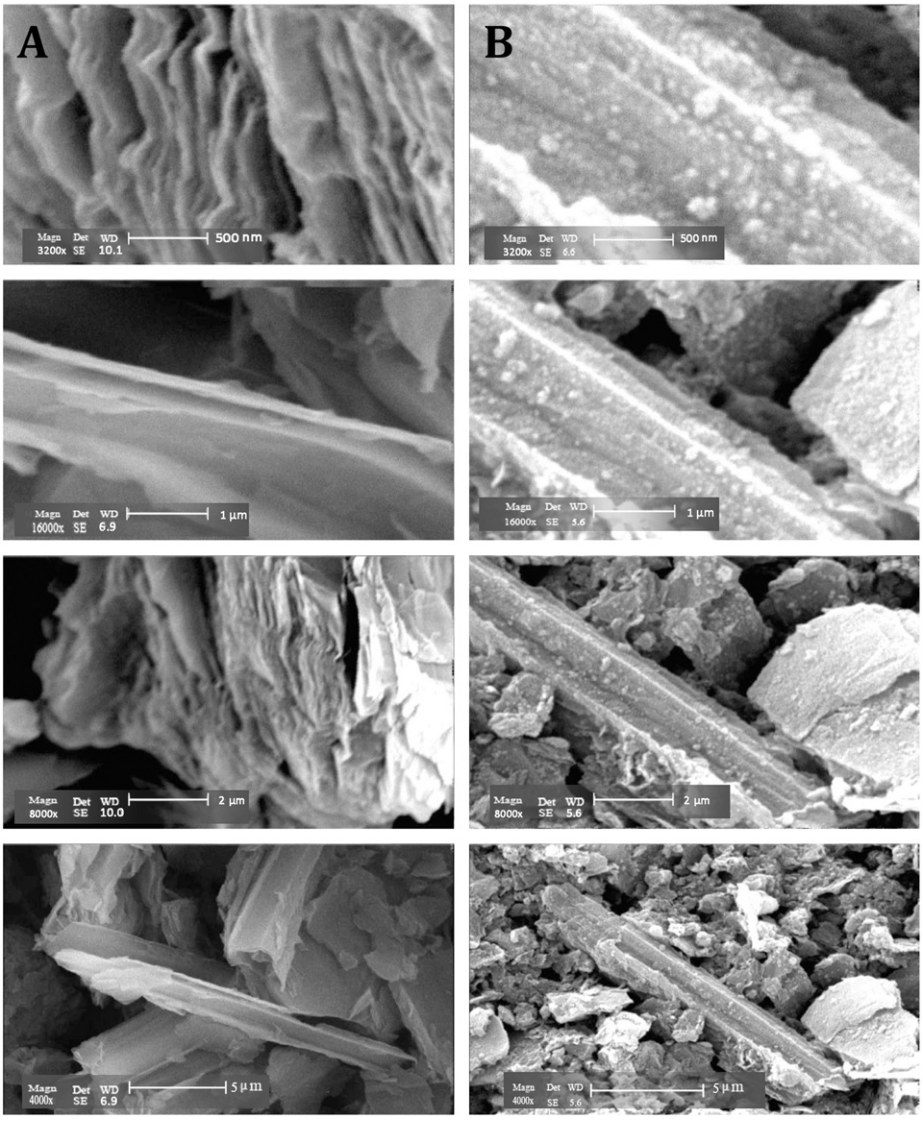

Fig. 1. SEM images of (A) EGO; and (B) EGO/Co_3O_4.

diffraction (XRD) analyses was carried out with a Bruker D_8/Advance X-ray diffractometer with Cu-K_a radiation.

2.3. Synthesis of exfoliated graphene oxide

Exfoliated graphene oxide was synthesized from graphite using the modified Hummers method as reported earlier [37]. Briefly, the process involves the treatment of cleaned graphite flakes of a certain size (~300 μm) with a mixture of sulphuric acid/nitric acid to obtain intercalated graphite. The low-density graphite is further oxidized using $KMnO_4$ and H_2O_2 to obtain a brown colored exfoliated graphene oxide (EGO) powder.

2.4. Synthesis of EGO–Co_3O_4 nanocomposite

500.0 mg of $Co(NO_3)_2$ was dissolved in 40.0 mL of 2-hexanol to form a red color solution. To this solution, 100 mg of EGO was added and dispersed by ultrasonication for 3 h. The mixture was then refluxed at 120 °C for 12 h [38]. After cooling down the mixture to room temperature, the as-synthesized product was filtered using a 0.45 μm filter and washed with ethanol (five times, each time with 10 mL) to remove any by-product before it was dried.

2.5. Preparation of Nafion/EGO–Co_3O_4 nanocomposite GCE

The GCE was successively polished to a mirror finish using a 0.3 μm alumina slurry followed by rinsing thoroughly with distilled water. After successive sonication in 1:1 ethanol and doubly distilled water (for 3 min), the electrode was rinsed in doubly distilled water and allowed to dry at room temperature. Then 30 μL of a suspension containing 3.0 mg EGO–Co_3O_4 nanocomposite in 10 mL ethanol was dropped on the pretreated GCE and dried at room temperature. Then, the Nafion film was prepared by dropping 10 μL of 5.0% Nafion on the EGO/Co_3O_4–GCE surface. The solvent was allowed to evaporate at room temperature. A Nafion film modified GCE was prepared using the same method.

3. Results and discussion

3.1. Characterization of Nafion/EGO–Co_3O_4 nanocomposite

Five different methods including SEM, XRD, FT-IR, CV, and EIS were used to investigate the characteristics of EGO–Co_3O_4 nanocomposite. SEM further investigated the morphology of EGO and EGO–Co_3O_4 nanocomposites. In Fig. 1A, the SEM images of graphene nanosheets illustrates the flake-like shapes of graphene oxide. Fig. 1B shows the graphene decorated with Co_3O_4 nanoparticles, confirms the graphene sheets covered with Co_3O_4 nanoparticles (Fig. 1B).

Fig. 2A shows XRD patterns of refined species of cobalt oxide. For this nanocomposite, four characteristic peaks occur at 2θ of 36.85°, 44.9°, 59.35°, and 65.1°. The diffraction peak at 2θ is equal to 36.85°. The diffractive peaks of Co_3O_4 are broadened, implying that the crystalline size of Co_3O_4 particles is quite small. The average particle size of Co_3O_4 nanoparticles was calculated as 30.2 nm based on peak width using the Scherrer equation.

Fig. 2B shows the IR absorption spectra of EGO–Co_3O_4 nanoparticles. The IR spectrum of the EGO sample displays one distinct band that originates from the stretching vibrations of the O–H bonds in 3400 cm^{-1} and a strong peak at 1550 cm^{-1} assigned to C–O stretching vibration of carboxylic and ester groups. The broad peak of Co_3O_4 displays single bands (584 and 507 cm^{-1}) likely to be associated with the metal-oxygen ions in octahedral holes, indicating an oxygen octahedral environment [39,40].

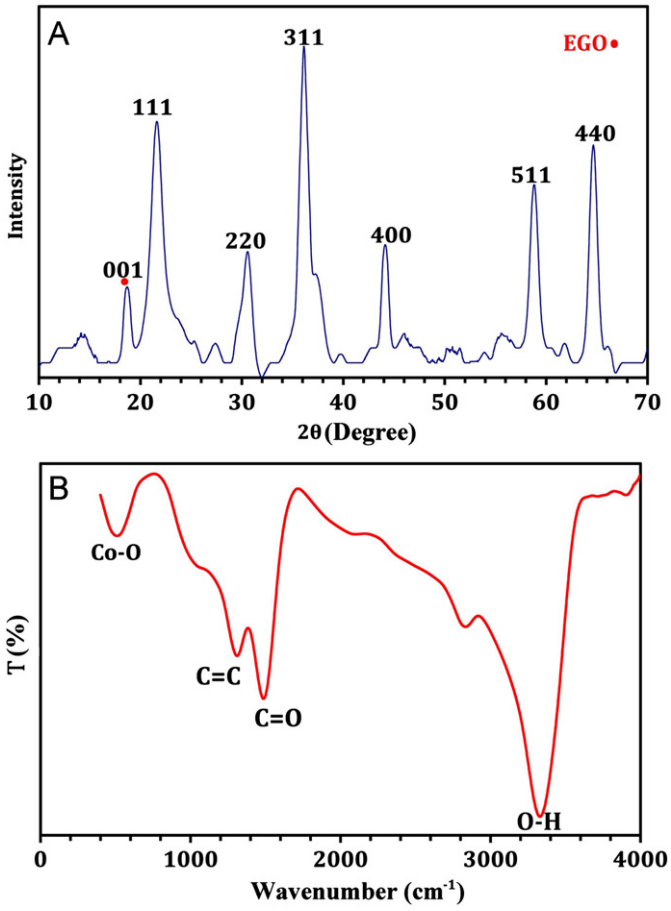

Fig. 2. (A) XRD patterns of EGO/Co_3O_4; (B) FT-IR of EGO/Co_3O_4.

Both CV and EIS techniques can be exploited to monitor the changes in the characteristics of GCE surface due to electrochemical oxidation as well as the modification with Nafion, EGO–Co_3O_4, and Nafion/EGO–Co_3O_4. Fig. 3A shows the cyclic voltammograms of the unmodified GCE (a), Nafion/GCE (b), EGO/Co_3O_4–GCE (c), and Nafion/EGO/Co_3O_4–GCE (d) obtained in 0.1 mmol L^{-1} $Fe(CN)_6^{3-}$ solution. An unmodified GCE showed a couple of well-defined redox peaks with a peak-to-peak separation (ΔE_p) of 81 mV. When the electrode was coated with Nafion, the peak currents decreased to a considerable extent. Moreover, the peak potential separations increased compared to those of the unmodified electrode. The negatively charged Nafion on the surface of the electrode developed at neutral pH levels. Consequently, the diffusion of ferrocyanide ions to the electrode surface was rarely ever blocked [41]. Nevertheless, after EGO/Co_3O_4 was immobilized on GCE, the redox peak current increased compared to GCE, indicating that EGO/Co_3O_4 can effectively increase the electron transfer rate due to its upstanding electric conductivity. Finally, after Nafion was immobilized on EGO/Co_3O_4–GCE, the redox peak current increased significantly compared to the case of GCE but decreased compared to the case of EGO/Co_3O_4–GCE. On the other hand, the electroactive surface area is estimated from the Randles–Sevcik equation [42] to be 0.068 cm^2 for the unmodified GCE and 0.134 cm^2 for Nafion/EGO/Co_3O_4–GCE. This indicates that Nafion/EGO/Co_3O_4–GCE may have better electrochemical reactivity than either the unmodified GCE or Nafion/GCE. For further characterization of the modified electrode, AC impedance spectroscopy was used too. Fig. 3B shows the Nyquist diagrams of electron transfer kinetics for a redox probe at the unmodified GCE, Nafion/GCE, EGO/Co_3O_4–GCE, and Nafion/EGO/Co_3O_4–GCE in

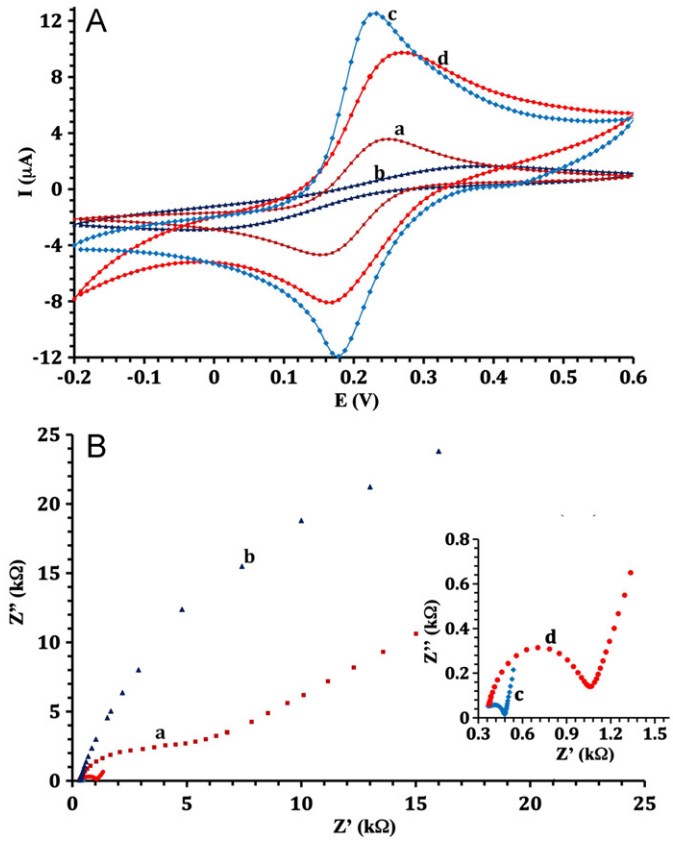

Fig. 3. Characterization of the sensing interface by (A) CV, and (B) EIS; (a): Unmodified GCE, (b): Nafion/GCE, (c): EGO/Co_3O_4–GCE, and (d): Nafion/EGO/Co_3O_4–GCE.

0.1 mmol L^{-1} $[Fe(CN)_6]^{3-}$. It can be seen that a small, well-defined semi-circle obtained at higher frequencies at the unmodified GCE, indicating small interface impedance. When Nafion was deposited on the surface of GCE, the impedance values increased drastically. This phenomenon could be attributed to the Nafion film itself, which introduces a resistance into the electrode/solution system. However, the electron resistance of the electrode decreased remarkably after EGO/Co_3O_4 was immobilized on the electrode surface, suggesting the excellent electroconductivity of the EGO/Co_3O_4 nanocomposite.

3.2. Electrochemical properties of the Nafion/EGO/Co_3O_4 nanocomposite on GCE

The electrochemical properties of Nafion/EGO/Co_3O_4 nanocomposite on the electrode surface were examined by recording cyclic voltammograms of the modified electrode in an alkaline solution (pH 12) (not shown). We observed a voltammogram similar to the reported in the literature [43]. These results can be attributed to the conversion between four different cobalt oxidation phases of $Co(OH)_2$, Co_3O_4, CoOOH, and CoO_2 which are stable at an alkaline pH [44]. As shown, two oxidation peaks were observed at 0.175 and 0.545 V during the positive potential scan. Peak I at 0.180 V corresponds to Co_3O_4 formation via the following reaction [45].

$$3Co(OH)_2 + 2OH^- \rightarrow Co_3O_4 + 4H_2O + 2e^- \quad (1)$$

This is while the peak II at 0.460 V can be assigned to CoOOH formation as a result of oxidation of $Co(OH)_2$ or the previously formed Co_3O_4.

$$Co(OH)_2 + OH^- \rightarrow CoOOH + H_2O + e^- \quad (2)$$

$$Co_3O_4 + H_2O + OH^- \rightarrow 3CoOOH + e^- \quad (3)$$

During the cathodic scan, two reduction peaks were observed at 0.420 and 0.150 V, corresponding to the reduction of various cobalt oxide species formed during the positive sweep.

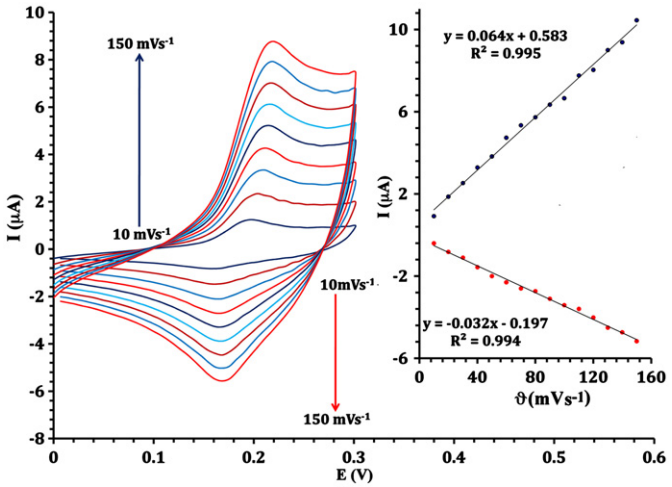

Fig. 4. Cyclic voltammograms of Nafion/EGO/Co_3O_4–modified GCE at different solution pH (4–12). Inset: Plot of the peaks current (anodic peak, and cathodic peak) vs. pH at scan rate of 50 mV s^{-1}.

Fig. 4 shows recording cyclic voltammograms of the modified electrode in the buffer solution (pH 12.0) at different scan rates. As can be seen, there is a linear relation between the anodic and/or cathodic peaks current and the scan rate. The ratio of the cathodic to the anodic peaks current and the peak potential of the waves are practically independent of the scan rate. Thus, the overall redox process confined at the electrode surface can be considered to be relatively fast on the voltammetric time scale. This result indicates that a surface confined redox process corresponds to a rapid conversion of a surface film without diffusion or kinetically controlled reaction step. Based on the Laviron theory, the values for (k_s) and (α) were calculated to be about 0.24 s^{-1} and 0.51, respectively [46,47]. The large value of the electron transfer rate constant indicates the high capability of cobalt oxide nanoparticles in the electron transfer process.

The effect of pH on the electrochemical behavior of the Nafion/EGO/Co_3O_4 modified GCE was investigated. The cyclic voltammetry response of the modified electrode at different pH levels of the solution is shown in Fig. 5. As can be seen, well-defined cyclic voltammograms are observed for a wide pH range. The peak potentials are shifted to less positive values with increasing the pH values while good linear relations are established between the E_{pa} and the solution pH; with increasing the pH levels, however, a change is observed in the slope, which can be related to the non-equal numbers of protons and electrons in the electrode reaction process at pH levels higher than 9.0 (Fig. 5, inset). Moreover, no peak currents are observed at pH values below 4.0 due to the solution of cobalt oxide nanoparticles [48]. Therefore, this modified electrode can be used at a wide range of pH values from 4.0 to 12.0 for electroanalytical detection methods or other applications.

3.3. Electrocatalytic oxidation of H_2O_2 at Nafion/EGO–Co_3O_4 nanocomposite–GCE

Biosensors developed for medical biodiagnostic applications typically use enzymes for the catalytically generation of a redox

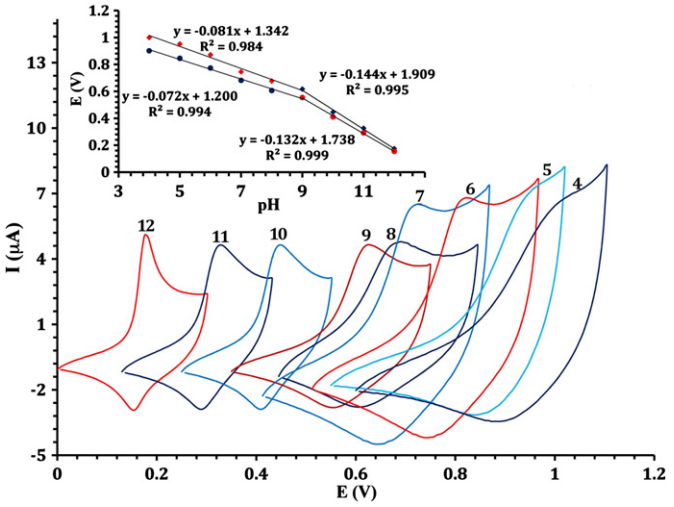

Fig. 5. Cyclic voltammetry response of GCE modified with Nafion/EGO/Co_3O_4 at pH 12.0 at different scan rates; From inner to outer: 10, 20, 30, 40, 50, 60, 70, 80, 90, 100, 110, 120, 130, 140 and 150 mV s^{-1}. Inset: Plot of the peaks current (anodic peak, and cathodic peak) vs. the scan rate.

active product such as hydrogen peroxide, which can be electrochemically detected via amperometry or coulometry. Therefore, there is a challenge for hydrogen peroxide detection at low concentration levels, especially in buffer solution with biological pH levels. In order to verify the electrocatalytic activity of the modified electrode for the oxidation of hydrogen peroxide, the electrochemical experiments were conducted in the presence of hydrogen peroxide. Fig. 6A, and B show the cyclic voltammograms of Nafion/EGO/Co_3O_4–GCE (A (a and b)), Nafion/Co_3O_4–GCE (B (b and c)), Nafion/EGO–GCE (A (c and d)) and unmodified GCE (B (d and e)) in the presence of 1.0 mmol L^{-1} H_2O_2 (A-a, A-c, B-b, and B-d) and in the absence of H_2O_2 (A-b, A-d, B-c, and B-e) at pH 7.4. As shown, no redox responses of H_2O_2 can be seen in the potential range from 0.30 to 1.20 V for Nafion/EGO–GCE and for unmodified GCE. However, at Nafion/Co_3O_4–GCE and at Nafion/EGO/Co_3O_4-GC electrode, the oxidation current of the Co_3O_4 is greatly enhanced due to the catalytic oxidation of hydrogen peroxide, while the reduction peak has largely disappeared. The decreasing in the overvoltage and increasing in the peak current of oxidation of hydrogen peroxide confirm that the exfoliated graphene oxide–Co_3O_4 nanocomposite has a high catalytic capability for H_2O_2 oxidation. Therefore, the cobalt oxide nanoparticles are suitable as mediator for shuttling electrons between hydrogen peroxide and GCE and for facilitating electrochemical regeneration following electron exchange with H_2O_2.

In order to optimize the electrocatalytic response of the modified electrode for H_2O_2 oxidation, the effect of pH on the catalytic oxidation behavior was investigated. The cyclic voltammograms of the modified electrode in 0.50 mmol L^{-1} H_2O_2 at different pH values were recorded (not shown). The results showed that at pH values ranging from 4.0 to 12.0, the modified electrode showed an electrocatalytic activity. However, higher peaks current were observed at pH levels of 6.0–7.4 and its reached to maximum value at pH 7.4. The oxidation of cobalt oxide and hydrogen peroxide are pH dependent. Therefore, the peak current and potential changed with changing the solution pH. Additionally, the peaks potential shifted to higher positive potentials with decreasing the solution pH. Since the modified electrode showed an excellent response to trace amounts of H_2O_2 at physiological pH values of 6.0–8.0, it can be concluded that it is capable of being used for the detection of hydrogen peroxide generated catalytically by enzymatic reactions.

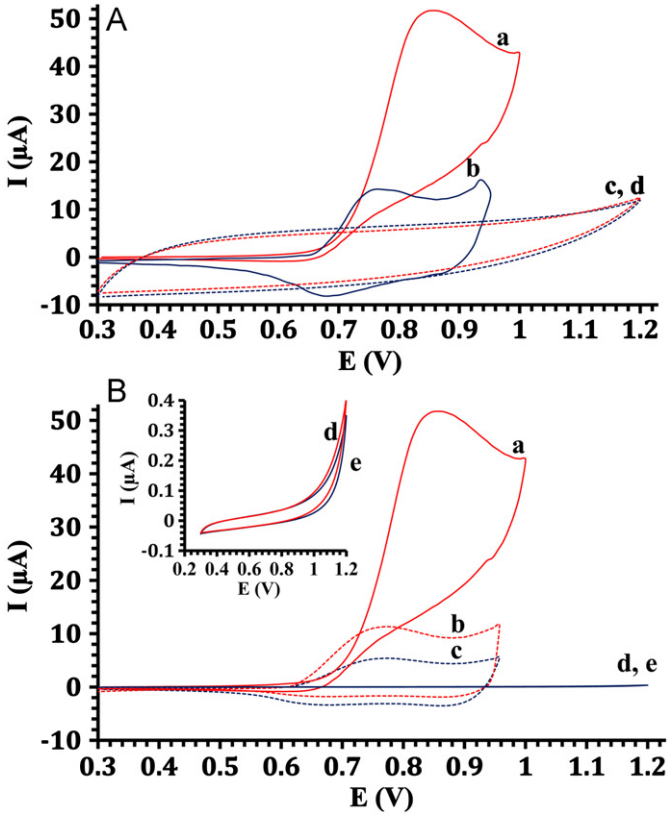

Fig. 6. A and B show the cyclic voltammograms of Nafion/EGO/Co_3O_4–GCE (A (a and b)) Nafion/Co_3O_4–GCE (B (b and c)), Nafion/EGO–GCE (A (c and d)) and unmodified GCE (B (d and e)) in the presence of 1.0 mmol L^{-1} H_2O_2 (A-a, A-c, B-b, and B-d) and in the absence of H_2O_2 (A-b, A-d, B-c, and B-e) at the buffer solution (pH 7.4) with scan rate of 50 mV s^{-1}.

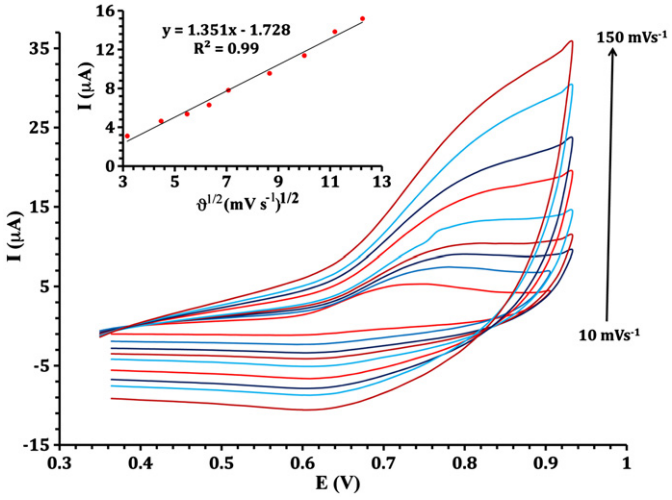

Fig. 7. CVs of 0.50 mmol L^{-1} H_2O_2 on Nafion/EGO/Co_3O_4–GCE at different scan rates from 10 to 150 mV s^{-1}. Inset: Plot of the oxidation peak current vs. square root of the scan rate.

By recording cyclic voltammograms of 0.50 mmol L^{-1} H_2O_2 solution at different scan rates (Fig. 7), the peak current for anodic oxidation of H_2O_2 was found to be proportional to the square root of the scan rate (Fig. 7, inset). However, at higher scan rates, hysteresis and anodic peak current appeared. This may be attributed to the fact that at the fast scan rate, Co_3O_4 was not completely reduced, leading to the reduction product that donates

electron transfer to H_2O_2 restrained in the time required for the scan. The results indicate that the electrocatalytic process was controlled by H_2O_2 diffusion to the electrode/solution interface and dependent on H_2O_2 concentration, which was ideal for quantitative applications. Furthermore, the peak potential for the catalytic oxidation of H_2O_2 shifted to more positive values with increasing the scan rate, suggesting that there was a kinetic limitation in the reaction between the redox sites of Co_3O_4 and H_2O_2.

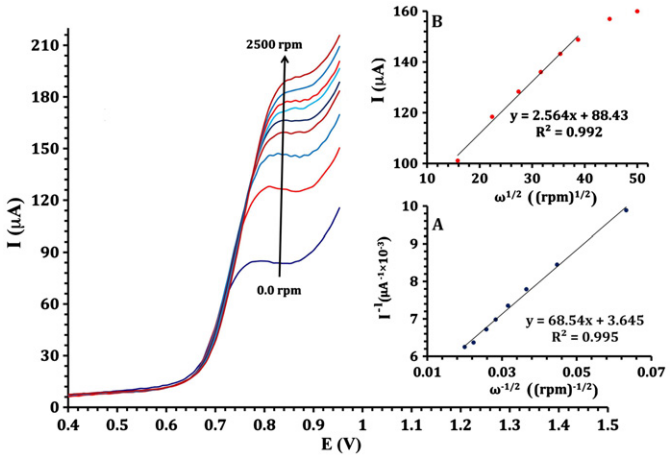

Fig. 8. Hydrodynamic voltammograms of 100 μmol L^{-1} H_2O_2 at the surface of Nafion/EGO/Co_3O_4 modified electrode in 0.1 mol L^{-1} PBS at various rotating speeds over a range of 0–2500 rpm. Koutecky–Levich plot (inset A) and Levich plot (inset B) of the hydrodynamic voltammograms.

3.4. Hydrodynamic voltammetric studies at rotating disk electrode

The hydrodynamic voltammograms of H_2O_2 on the surface of Nafion/EGO/Co_3O_4–modified GCE were recorded at different rotation rates over the range of 0–2500 rpm (Fig. 8). However, under these conditions and based on the hydrodynamic voltammograms, a linear correlation exists between the inverse of the limiting current and the inverse of the square root of the rotating speed (Koutecky–Levich equation), as illustrated in the inset of Fig. 8 (inset A). This equation can be formulated as follows:

$$1/I_{\mathrm{lim}} = 1/I_k + 1/\left(0.62nFA\upsilon^{-1/6}D^{2/3}C\omega^{1/2}\right) \quad (4)$$

where I_k is the plateau current limited by the kinetic step, C is the bulk concentration of H_2O_2 in solution, υ is the kinematic viscosity, and ω is the angular frequency. The diffusion coefficient of H_2O_2 under these conditions was calculated from the sleep of Koutecky–Levich plot to be 1.14×10^{-6} cm^2 s^{-1}. Other symbols have their usual meanings. The limiting currents at different rotating rates versus the square root of the rotating rate were plotted as shown in the inset of Fig. 8, inset B (Levich plot). Contrary to the expectation arising from the Levich equation, it is seen in the inset of Fig. 8 (inset B) that this plot is not linear and tends to level off at higher rotation rates. This nonlinearity suggests a kinetic limitation in the coupled chemical reaction. Hence, it may be concluded that the rate-determining step in this process is related to the oxidation of hydrogen peroxide at the modified electrode, and that this would be evidence for the two-electron mechanisms that follow:

$$Co_3O_4 + H_2O + OH^- \rightarrow 3CoOOH + e^- \quad (5)$$

$$6CoOOH + H_2O_2 \xrightarrow{K_{cat}} 2Co_3O_4 + O_2 + 4H^+ \quad (6)$$

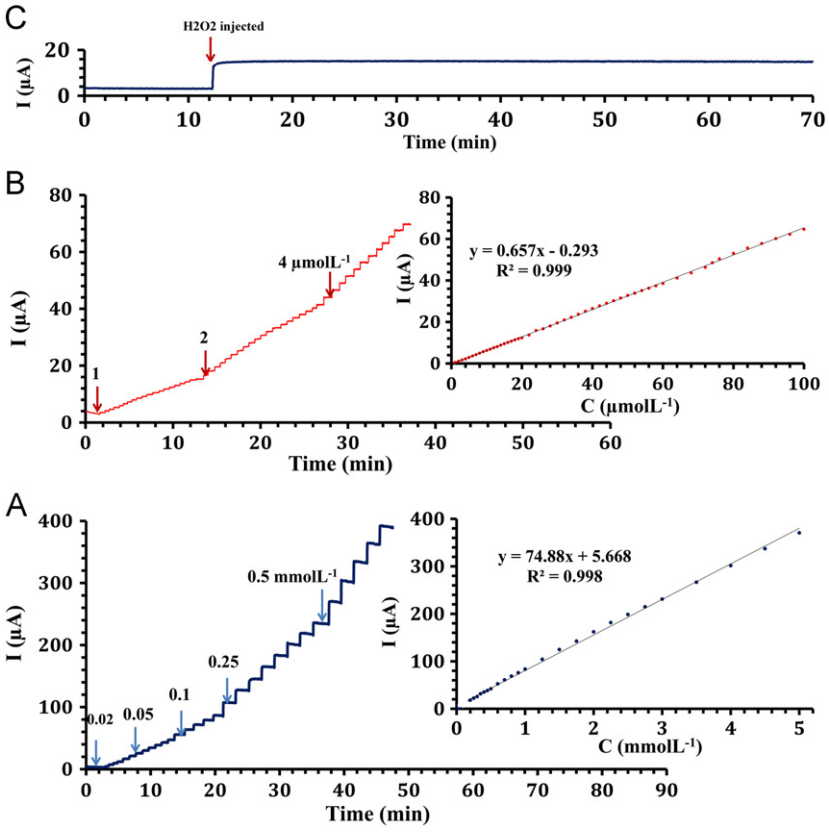

Fig. 9. Typical amperometric responses of rotating Nafion/EGO/Co_3O_4–GCE (with rotation speed of 1800 rpm) held at 0.76 V in the buffer solution (pH 7.4) after successive addition of H_2O_2; (A) 0.020–0.50 mmol L^{-1} H_2O_2; (B): 1.0, 2.0 and 4.0 μmol L^{-1} H_2O_2; (C) Chronoamperogram of 100 μmol L^{-1} H_2O_2 during long time (60 min). Insets A and B: The calibration curves for the amperometric determination of H_2O_2 using the modified electrode.

3.5. Amperometric detection of H_2O_2 at the modified Nafion/EGO–Co_3O_4 nanocomposite–GCE

The amperometric responses of Nafion/EGO/Co_3O_4–GCE with an applied potential at +760 mV in 0.01 mol L^{-1} PBS (pH 7.4) for successive addition of H_2O_2 are presented in Fig. 9A and B. The time required to reach 95% of the maximum steady-state current is within 4 s (Fig. 9C), indicating that the process is fast and that it could well catalyze the oxidation of H_2O_2. Insets in Fig. 9A and B are the calibration curves of the current vs. H_2O_2 concentration. These figures show that the amperometric currents increased linearly with H_2O_2 concentration from 1.0 to 100.0 μmol L^{-1} and obeying the linear regression equation of $I(\mu A)=0.657C(\mu mol\ L^{-1})-0.293$ ($R^2=0.999$, $n=50$), while the linear regression equation for 100.0 μmol L^{-1} to 5.0 mmol L^{-1} H_2O_2 was $I(\mu A)=74.880C(mmol\ L^{-1})+5.668$ ($R^2=0.998$, $n=28$), indicating that the regression line is very well fitted with the experimental data.

The detection limit (S/N=3) and the sensitivity of the amperometric method were 0.3 μmol L^{-1} and 560 μA $mmol^{-1}$ L cm^{-2}, respectively [49]. Table 1 compares the performance of Nafion/EGO/Co_3O_4–GCE sensor with those of other non-enzymatic H_2O_2 reported elsewhere. From Table 1, it is clear that the detection limit, linear calibration range, and sensitivity of the new sensor are comparable and even better than those obtained by other modified electrodes [50–59] based on metal, metal oxide nanoparticles and nanocomposites.

3.6. Stability and reproducibility of the H_2O_2 sensor

Fig. 9C shows the amperometric response of 100 μmol L^{-1} hydrogen peroxide during an experiment prolonged for 60 min. Clearly, the response remains stable throughout the experiment (a decrease of only 1% observed in the current), indicating no inhibition effect by H_2O_2 and its oxidation products for the modified electrode surface. Another attractive feature of Nafion/EGO/Co_3O_4–GCE is the relative standard deviation (R.S.D.) determined by 6 successive assays of 100 μmol L^{-1} H_2O_2 that was found to be 4.3%. Therefore, the modified electrode has an excellent and stable operation for the measurement of hydrogen peroxide. When the modified electrode was stored at room temperature for two weeks, it retained more than 96.6% of its initial sensitivity to the oxidation of H_2O_2, showing that the modified electrode is of a good, long-term stability.

The fabrication reproducibility of the modified electrode was investigated by preparing four sensors independently in four days using the same procedure, and four replicate measurements were made on the same samples by the modified electrode (to obtain a within-modified electrodes variation ($S_W=0.68$) and between-modified electrodes variation ($S_B=0.92$)). To test whether significantly greater or not, a one-sided F-test is used. The critical value of F ($F_{3,12}$) is equal to 3.49 and the calculate value of $F_{3,12}$ was 1.84 ($P=0.05$). Since the calculated value of the F was smaller than the critical value, therefore, null hypothesis accepted. The results indicate the excellent reproducibility and repeatability of the modified electrode.

4. Interference study

One of the most important challenges faced with in practical applications of amperometric sensors is minimizing the effect of interfering species possibly present in real samples. The selectivity and anti-interference ability of the Nafion/EGO/Co_3O_4–GCE was investigated for an interference/analyte concentration ratio in the range of 1:1 (100 μmol L^{-1}) to 50:1. The conclusion to be drawn from the results summarized in Table 2 is that the method is free from interference by most foreign substances. The catalytic selectivity is enhanced by the low working potential (+0.76 V). Maine interference compounds in the determination of H_2O_2 are glucose (Glu), ascorbic acid (AA) and uric acid (UA). The results of our studied showed that the new sensor is free from of these interfering compounds. This is due to the fact that Nafion (that

Table 2
Effect of interfering species on the amperometric determination of 100.0 μmol L^{-1} H_2O_2 with Nafion/EGO–Co_3O_4–GCE.

Species	Concentration ratio of H_2O_2:Species	Current ratio
Uric acid	1:5	1.06
Cysteine	1:5	0.87
Thioguanine	1:5	0.92
Ascorbic acid	1:10	1.03
Lucien	1:20	1.02
Glycine	1:20	1.03
Citric acid	1:30	0.97
Glucose	1:50	1
Histidine	1:50	1
Tartaric acid	1:50	1
CO_3^{2-}	1:50	1
Ca^{2+}	1:50	1
Epinephrine	1:50	1
Captopril	1:50	1

Table 1
Analytical parameters for several modified electrodes for determination of hydrogen peroxide.

H_2O_2 sensor	Detection limit (μmol L^{-1})	Linear range (μmol L^{-1})	Sensitivity (μA $mmol^{-1}$ L cm^{-2})	Interference			Reference
				Tolerance limit ($mmol^{-1}$ L)			
				Glu	AA	UA	
Graphene/AuNPs/CS–Au	–	200–4200	99.5	Not reported	Not reported	Not reported	50
RGO/Fe_3O_4	3.2	100–6000	688	2	2	Not reported	51
Graphene–MWCNTs	9.4	20–2100	15	Not reported	Not reported	Not reported	52
H-GNs	0.2	0.5–400	Not reported	Not reported	0.4	0.4	53
Graphene–Pt	0.5	2–710	Not reported	Not reported	0.05	0.05	54
Pt/CNFE	0.6	1–800	Not reported	Not reported	0.1	0.1	55
MnO_2/VACNTs	0.8	1.2–1800	1.04×10^5	0.1	Not reported	0.1	56
Graphene-CS/PB	0.2	10–400	816	Not reported	0.1	Not reported	57
RGO/ZnO	0.02	1–22.5	1.35×10^4	1	1	Not reported	58
$LaNi_{0.5}Ti_{0.5}O_3/CoFe_2O_4$	0.02	0.1–8200	3.2	Not reported	Not reported	Not reported	59
Nafion/EGO/Co_3O_4–GC	0.3	1–5000	560	5	1	0.5	This Work

Glu: Glucose, AA: Ascorbic acid, UA: Uric acid, GCE: Glassy carbon electrode; EGO: Exfoliated graphene oxide; RGO Reduced graphene oxide; H-GNs: Hemin functionalized graphene nanosheets; CF: Carbon fiber; VACNTs: Vertically aligned multiwall carbon nanotubes; PB/CS: Prussian blue/chitosan.

presence at the sensor surface) is a perfluorinated anionic polyelectrolyte. On the other hand, the predominate form of UA and AA at the optimum pH (7.4) in anionic form. Thus, excess of these substances could not interfere in the determination of H_2O_2.

5. Real sample analysis

The determination of H_2O2 in ultra-high-temperature (UHT) processed milk was carried out to verify the practical application of the proposed electrochemical sensor. For this purpose, 100 μL of the milk sample was added to 20.0 mL 0.1 mol L^{-1} PBS solution (pH 7.4) and the current response was recorded at +0.76 V. H_2O_2 concentrations in the milk sample was determined to be 520 ± 17.9 mg L^{-1} ($n=10$). Recovery of H_2O_2 determined by the standard addition method was recorded at 104.7%. These amperometric results are consistent with those obtained by titration in acidic media ($2MnO_4^- + 5H_2O_2 + 6H^+ \rightarrow 2Mn^{2+} + 5O_2 + 8H_2O$) [3]. Furthermore, the desirable recovery of the Nafion/EGO–Co_3O_4 modified GCE verifies the suitability of the proposed sensor for real sample analysis.

6. Conclusions

In summary, a novel and biocompatible Nafion/EGO/Co_3O_4 nanocomposite was successfully prepared and applied for electrochemical sensor fabrication. The structural and surface morphology investigations revealed that the ultrathin film is continuous and uniform with long range stacking order in the normal direction of the substrate. The Nafion/EGO/Co_3O_4 nanocomposite modified electrode showed a high electrocatalytic activity toward H_2O_2. The synergistic effect of exfoliated graphene oxide and Co_3O_4 may promote electrocalalysis toward H_2O_2. In view of its inherent selectivity in combination with its great operational stability, the proposed sensor shows promising properties for use in real samples with minimal sample preparation. It is obvious that the low overpotential for H_2O_2 detection at this electrode excludes the effects due to interference, indicating the good selectivity of the Nafion/EGO/Co_3O_4 nanocomposite. In addition, the modified electrode is characterized not only by its good sensitivity and fast response, but also by its acceptable stability, high selectivity and reproducibility toward H_2O_2 determination. The proposed sensor has long linear dynamic range better selectivity (free from interferences especially AA, UA and glucose).

Acknowledgment

Thanks are due to the Iranian Nanotechnology Initiative, the Research Council of Isfahan University of Technology and Centre of Excellence in Sensor and Green Chemistry for supporting of this work.

Reference

[1] Y. Usui, K. Sato, M. Tanaka, Angew. Chem. 42 (2003) 5623–5625.
[2] I. Alpat, S.K. Alpat, Z. Dursun, A. Telefoncu, J. Appl. Electrochem. 39 (2009) 971–977.
[3] A.I. Vogel, Textbook of Quantitative Chemical Analysis, Longman, UK, 1989.
[4] F.A. Armstrong, A.M. Lanon, J. Am. Chem. Soc. 109 (1987) 7211–7212.
[5] M. Darder, K. Takada, F. Pariente, E. Lorenzo, H.D. Abruna, Anal. Chem. 71 (1999) 5530–5537.
[6] G. Xu, S. Dong, Electroanalysis 11 (1999) 1180–1184.
[7] W. Yang, Y. Li, Y. Bai, C. Sun, Sens. Actuators, B 115 (2006) 42–48.
[8] C. Liu, J. Hu, Z. Chen, Biosens. Bioelectron. 24 (2009) 2149–2154.
[9] X. Feng, Y. Liu, Q. Kong, J. Ye, X. Chen, J. Hu, Z. Chen, J. Solid State Electrochem. 14 (2010) 923–930.
[10] X. Miao, R. Yuan, Y. Chai, Y. Shi, Y. Yuan, J. Electroanal. Chem. 612 (2008) 157–163.
[11] A. Safavi, N. Maleki, E. Farjamia, Electroanalysis 21 (2009) 1533–1538.
[12] Z. Taha, J. Wang, Electroanalysis 3 (1991) 215–219.
[13] X. He, C. Hu, H. Liu, G. Du, Y. Xi, Y. Jiang, Sens. Actuators, B 144 (2010) 289–294.
[14] J. Huang, D. Wang, H. Hou, T. You, Adv. Funct. Mater. 18 (2008) 441–448.
[15] S. Hrapovic, Y. Liu, K.B. Male, J.H.T. Luong, Anal. Chem. 76 (2004) 1083–1088.
[16] H. Jeong, M.S. Ahmed, S. Jeon, J. Nanosci. Nanotechnol. 11 (2011) 987–993.
[17] S. Daniel, T.P. Rao, K.S. Rao, S.U. Rani, G.R.K. Naidu, H.Y. Lee, T. Kawai, Sens. Actuators, B 122 (2007) 672–682.
[18] D.M. Guldi, G.M.A. Rahman, F. Zerbetto, M. Prato, Acc. Chem. Res. 38 (2005) 871–878.
[19] Y. Wang, Xi. Ma, Y. Wen, Y. Xing, Z. Zhang, H. Yang, Biosens. Bioelectron. 25 (2010) 2442–2446.
[20] S.F. Ding, W. Wei, G. Ch. Zhao, Electrochem. Commun. 9 (2007) 2202–2206.
[21] Z. Lu, Q. Huang, J.F. Rusling, J. Electroanal. Chem. 423 (1997) 59–66.
[22] K. Kalcher, Electroanalysis 2 (1990) 419–433.
[23] K. Kalcher, J.M. Kauffmann, J. Wang, I. Svancara, K. Vytras, C. Neuhold, Z. Yang, Electroanalysis 7 (1995) 5–22.
[24] C.M. Welch, C.E. Banks, A.O. Simm, R.G. Compton, Anal. Bioanal. Chem. 382 (2005) 12–21.
[25] J. Li, Q. Yu, T. Peng, Anal. Sci. 21 (2005) 377–382.
[26] W. Yang, Y. Li, Y. Bai, C. Sun, Sens. Actuators, B 115 (2006) 42–48.
[27] H. Elzanowska, E. Abu-Irhayem, B. Skrzynecka, V.I. Birss, Electroanalysis 16 (2004) 478–490.
[28] J. Wang, G. Rivas, M. Chicharro, J. Electroanal. Chem. 439 (1997) 55–61.
[29] J. Wang, L. Angnes, Anal. Chem. 64 (1992) 456–459.
[30] X. Cai, B. Ogorevc, G. Tavčar, J. Wang, Analyst 120 (1995) 2579–2583.
[31] J. Wang, L. Fang, D. Lopez, H. Tobias, Anal. Lett. 26 (1993) 1819–1830.
[32] L.F. Fan, X.Q. Wu, M.D. Guo, Y.T. Gao, Electrochim. Acta 52 (2007) 3654–3659.
[33] M. Jafarian, M.G. Mahjani, H. Heli, F. Gobal, H. Khajehsharifi, M.H. Hamedi, Electrochim. Acta 48 (2003) 3423–3429.
[34] N. Varghese, U. Mogera, A. Govindaraj, A. Das, P.K. Maiti, A.K. Sood, C.N.R. Ra, Chem. Phys. Chem. 10 (2009) 206–210.
[35] C.S. Shan, H.F. Yang, J.F. Song, D.X. Han, A. Ivaska, L. Niu, Anal. Chem. 81 (2009) 2378–2382.
[36] Y. Xu, H. Bai, G.W. Lu, C. Li, G.Q. Shi, J. Am. Chem. Soc. 130 (2008) 5856–5857.
[37] P. Ramesh, S. Sampath, J. Colloid Interface Sci. 274 (2004) 95–102.
[38] C. Xiu, X. Wang, J. Zhu, X. Yang, L. Lu, J. Mater. Chem. 18 (2008) 5625–5629.
[39] S.G. Christoskova, M. Stoyanova, M. Georgieva, D. Mehandjiev, Mater. Chem. Phys. 60 (1999) 39–43.
[40] Y. Okamoto, H. Nakano, T. Imanaka, S. Teranishi, Bull. Chem. Soc. Jpn. 48 (1975) 1163–1168.
[41] H. Chen, Y. Wang, Y. Liu, L. Qi, S. Dong, Electrochem. Commun. 9 (2007) 469–474.
[42] J. Wang, Analytical Electrochemistry, third ed., Wiley-VCH, New York, 2006.
[43] C. Barbero, G.A. Planes, M.C. Miras, Electrochem. Commun. 3 (2001) 113–116.
[44] I.G. Casella, J. Electroanal. Chem. 520 (2002) 119–125.
[45] E.A. McNally, I. Zhitomirsky, D.S. Wilkinson, Mater. Chem. Phys. 91 (2005) 391–398.
[46] E. Laviron, J. Electroanal. Chem. 52 (1974) 355–363.
[47] E. Laviron, J. Electroanal. Chem. 101 (1979) 19–28.
[48] S. Floate, M. Hyde, R.G. Compton, J. Electroanal. Chem. 523 (2002) 49–63.
[49] J.N. Miller, J.C. Miller, Statistics and Chemometrics for Analytical Chemistry, fifth ed., Pearson Education Limited, 2005.
[50] C. Shan, H. Yang, D. Han, Q. Zhang, A. Ivaska, L. Niu, Biosens. Bioelectron. 25 (2010) 1070–1074.
[51] Y. Yea, T. Kong, X. Yuc, Y. Wuc, K. Zhang, X. Wang, Talanta 89 (2012) 417–421.
[52] S. Wooa, Y.R. Kim, T.D. Chung, Y. Piao, H. Kim, Electrochim. Acta 59 (2012) 509–514.
[53] Y. Guo, J. Li, Sh. Dong, Sens. Actuators, B 160 (2011) 295–300.
[54] F. Xu, Y. Sun, Y. Zhang, Y. Shi, Z. Wen, Z. Li, Electrochem. Commun. 13 (2011) 1131–1134.
[55] Y. Liua, D. Wanga, L. Xua, H. Houb, T. You, Biosens. Bioelectron. 26 (2011) 4585–4590.
[56] B. Xu, M. Ye, Y. Yu, W. Zhang, Anal. Chim. Acta 674 (2010) 20–26.
[57] J.H. Yang, N. Myoung, H.G. Hong, Electrochim. Acta 81 (2012) 37–43.
[58] S. Palanisamy, Sh.M. Chen, R. Sarawathi, Sens. Actuators, B 166–167 (2012) 372–377.
[59] D. Ye, Y. Xu, L. Luo, Y. Ding, Y. Wang, X. Liu, L. Xing, J. Peng, Colloids Surf., B 89 (2012) 10–14.